JOURNAL OF GEOPHYSICAL RESEARCH, VOL. 108, NO. B2, 2087, doi:10.1029/2001JB000456, 2003

A transient subduction zone slip episode in southwest Japan observed by the nationwide GPS array

Shin'ichi Miyazaki
Earthquake Research Institute, University of Tokyo, Tokyo, Japan

Jeffrey J. McGuire[1] and Paul Segall
Department of Geophysics, Stanford University, Stanford, California, USA

Received 13 February 2001; revised 9 August 2002; accepted 5 September 2002; published 11 February 2003.

[1] We investigate the spatiotemporal variation of fault slip on the subduction interface in southwest Japan following the two 1996 Hyuganada earthquakes (M 6.7) using continuous GPS observations. A silent thrust slip event has been reported by *Hirose et al.* [1999], following these earthquakes approximately 100 km to the north beneath the Bungo channel. We employ the Network Inversion Filter to rigorously invert for the fault slip distribution in space and time. The GPS time series is modeled as a sum of: (1) secular deformation; (2) coseismic station displacements; (3) transient fault slip; (4) random benchmark motion; (5) reference frame shifts; and (6) observational errors. Nonnegativity constraints effectively prohibit normal faulting on the subduction interface. Spatial and temporal smoothing parameters are estimated by the extended Kalman filter. The estimated fault slip-rate images postseismic slip following the two Hyuganada earthquakes. Slip associated with the silent thrust event began roughly 1 month after the second earthquake but initiated ~100 km to the northeast of the Hyuganada earthquakes. The slow event propagated southwest and downdip beneath the Bungo channel, lasting approximately 1 year with maximum slip-rates of 0.6 m/yr. The equivalent seismic moment was $M_W \sim 7.2$. We can rule out the possibility that slip propagated from the source region of the Hyuganada earthquakes to the location of the silent earthquake. However, the timing of the events suggests a causal connection, perhaps due to static stress transfer. This kind of transient event, or silent earthquake, may reflect different fault zone characteristics and may be responsible for accommodating strain that would otherwise be released in large earthquakes. *INDEX TERMS:* 1206 Geodesy and Gravity: Crustal movements—interplate (8155); 1242 Geodesy and Gravity: Seismic deformations (7205); 1243 Geodesy and Gravity: Space geodetic surveys; 8150 Tectonophysics: Plate boundary—general (3040); *KEYWORDS:* transient crustal deformation, GPS, network inversion filter

Citation: Miyazaki, S., J. J. McGuire, and P. Segall, A transient subduction zone slip episode in southwest Japan observed by the nationwide GPS array, *J. Geophys. Res.*, *108*(B2), 2087, doi:10.1029/2001JB000456, 2003.

1. Introduction

[2] The Japanese Islands have long suffered from great mega-thrust earthquakes. The Nankai Trough, where the Philippine Sea plate is subducting beneath southwest Japan at an annual rate of about 65 mm/yr [*Heki et al.*, 1999], has been the site of M ~ 8 class earthquakes every 100–200 years over the last one thousand years [e.g., *Ando*, 1975; *Sangawa*, 1993; *Kumagai*, 1996]. The 1944 Tonankai and the 1946 Nankaido earthquakes are the latest such events. Although the Nankai and Tonankai areas are known for great earthquakes, no such events are known to have occurred in the Hyuganada region along the east coast of Kyushu, where the largest historical event is the M7.5 1968 Hyuganada earthquake. The area is instead characterized by intermediate (M ~ 7) earthquakes [e.g., *Shiono et al.*, 1980].

[3] The Japanese nationwide GPS network, GEONET (GPS Earth Observation Network) [e.g., *Miyazaki et al.*, 1997] has helped to elucidate the interseismic crustal velocity field in southwest Japan. Inversion of these data suggests that the plate interface in the Nankai–Tonakai area is strongly coupled while the Hyuganada area is only weakly coupled [e.g., *Ito et al.*, 1999]. These two areas are separated by the Bungo Channel where the interseismic coupling may change abruptly, perhaps due to changes in fault zone constitutive properties or fault geometry.

[4] In the Hyuganada area, two thrust earthquakes, both $M_W = 6.7$, occurred on 19 October and 2 December 1996 [e.g., *Yagi et al.*, 1999, 2001]. Postseismic deformation similar to that following the 1994 Sanriku Haruka Oki earthquake [*Heki et al.*, 1997] might be expected to be

[1]Now at Department of Geology and Geophysics, Woods Hole Oceanographic Institution, Woods Hole, Massachusetts, USA.

0148-0227/03/2001JB000456$09.00

recorded by GEONET. In addition to the postseismic deformation, *Hirose et al.*, [1999] reported a "slow thrust slip event" that occurred beneath the Bungo Channel in 1997. This event is characterized by an extremely long duration of ~300 days. *Hirose et al.* [1999] modeled the transient signal with a trapezoidal source time function, and inverted the total displacement field to infer the net transient fault slip distribution. They concluded that the maximum fault slip was 0.18 m over a 60 × 60 km^2 area, corresponding to a seismic moment of 1.1×10^{19} Nm (corresponding to M_W 6.6).

[5] Previously, it had been almost impossible to retrieve the spatiotemporal history of fault slip in the period band of days to months, because data was limited to infrequent geodetic surveys. Permanent GPS networks offer a continuous record of the deformation field. Given the spatial density of modern networks, such as GEONET, we are able to infer the space–time evolution of fault slip during the interseismic period. *Segall and Matthews* [1997] proposed one method, the Network Inversion Filter (NIF), to retrieve the time dependent history of the slip distribution using continuous geodetic data.

[6] In the present paper, we employ a modified version of the NIF that accounts for errors in the GPS reference frame, and allows nonnegativity constraints and automatic determination of the spatial and temporal smoothing parameters (McGuire, J., and P. Segall, Imaging of aseismic slip transients recorded by dense geodetic networks, submitted to *Geophysical Journal International*, 2002, hereinafter referred to as McGuire and Segall, submitted manuscript, 2002). We apply the method to GEONET data in southwest Japan to estimate the spatiotemporal variation of afterslip following the two Hyuganada earthquakes and the silent thrust slip event. Since we focus on the first 1.5 years after the earthquakes, viscous-like relaxation of the lower crust is not expected to be the dominant process and is ignored in our analysis. Other time-dependent processes, such as poroelasticity are also not treated in this work. In addition to systematically studying the slow slip event, we investigate whether afterslip following the Hyuganada quakes propagated to the north, triggering the slow thrust event, or whether the slow earthquake nucleated independently of the Hyuganada earthquakes.

[7] *Ozawa et al.* [2001] also investigated the silent thrust event using related methods. Although their approach is similar to ours in that both employ Kalman Filtering methods based on the approach of *Segall and Matthews* [1997], the details are different. Specifically, the parameterization of fault geometry and slip-rate distribution, the time dependent slip model, regularization methods, and the treatment of seasonal variations in GPS time series, are all handled differently. Furthermore, we include a nonnegativity constraint on fault slip, and estimate the spatial and temporal smoothing parameters automatically in an extended Kalman Filter. *Ozawa et al.* [2001] showed, using nonlinear inversion, the net displacement field between April 1996 and February 1998 can be reasonably explained by slip on the Nankai Trough subduction interface beneath the Bungo Channel. Their time dependent results showed slip propagating from the source region of the Hyuganada earthquakes to the northeast and the Bungo Channel, although *Ozawa et al.* [2001] suggest that this may have been an artifact of oversmoothing in the inversion. We show here, using improved inversion methods, that the silent earthquake nucleated separately ~100 km to the northeast of the Hyuganada earthquakes and actually propagated back to the southwest. The intervening region between the high frequency and silent earthquakes did not experience transient slip during this time interval.

2. Data

[8] The Geographical Survey Institute of Japan (GSI) began to operate its nationwide GPS network on October 1994 [*Tsuji et al.*, 1995]. This first generation nationwide network was expanded to a denser network consisting of 610 permanent stations on April 1996, and the data analysis strategy was changed to that which had been used until early 2001. An outline of the daily analysis strategy is found by *Miyazaki et al.* [1997], and is reviewed briefly here.

[9] The entire data set is divided into three subnetworks based on different antenna-receiver types. Each subnetwork is processed separately using Bernese ver 4.1β software [*Rothacher and Malvert*, 1996]. GSI utilizes precise orbit information and Earth rotation parameters provided by the International GPS Service (IGS). The orbit and Earth rotation parameters are fixed to their a priori values, and station positions are estimated together with tropospheric zenith delays every three hours. The three subnetworks are combined by tightly constraining positions to their ITRF96 values [*Sillard et al.*, 1998] (at the 0.1 mm level) of three GPS stations in Tsukuba, which are present in all three subnetworks. This procedure prevents us from determining the correlations between stations in the separate subnetworks.

[10] We use a subset of the GEONET data from 4 September 1996 to 31 December 1999, covering Kyushu and the western part of Shikoku (Figure 1). The network is composed of Ashtech and Trimble stations, marked with diamonds and circles, (Figure 1), respectively. We treat these two subnetworks as two individual networks because of the lack of correlation between them in the position covariance matrices.

[11] It is known that GPS coordinate estimates can contain translational, rotational, and scale errors in their realization of the International Terrestrial Reference Frame (ITRF). In addition to these global errors, the GSI time series contain errors due to the tight constraints on the position of the Tsukuba GPS stations, which reveals different seasonal behavior (~2 cm in vertical amplitude) from other stations in eastern Asia [*Dong et al.*, 2002]. This may cause nontectonic benchmark motion at a site in Tsukuba to propagate into all stations within that GPS subnetwork.

[12] The formal uncertainties in the GSI position estimates are between 2 mm and 4 mm; however, these do not account for the reference frame errors described above. It is advantageous to use loosely constrained solutions from which one can estimate and remove reference frame errors [*Dong et al.*, 1998]. *Dong* [1999] (available at http://gipsy.jpl.nasa.gov/qoca) shows that tightly constrained solutions can be "deconstrained" by applying the transformation

$$\Sigma_{\mathbf{x}_{new}} = \left(\Sigma^{-1}_{\mathbf{x}_{old}} - A^{-1}_{old} + A^{-1}_{new}\right)^{-1} \quad (1)$$

$$\mathbf{x}_{new} = \Sigma_{\mathbf{x}_{new}} \Sigma^{-1}_{\mathbf{x}_{old}} \mathbf{x}_{old} \quad (2)$$

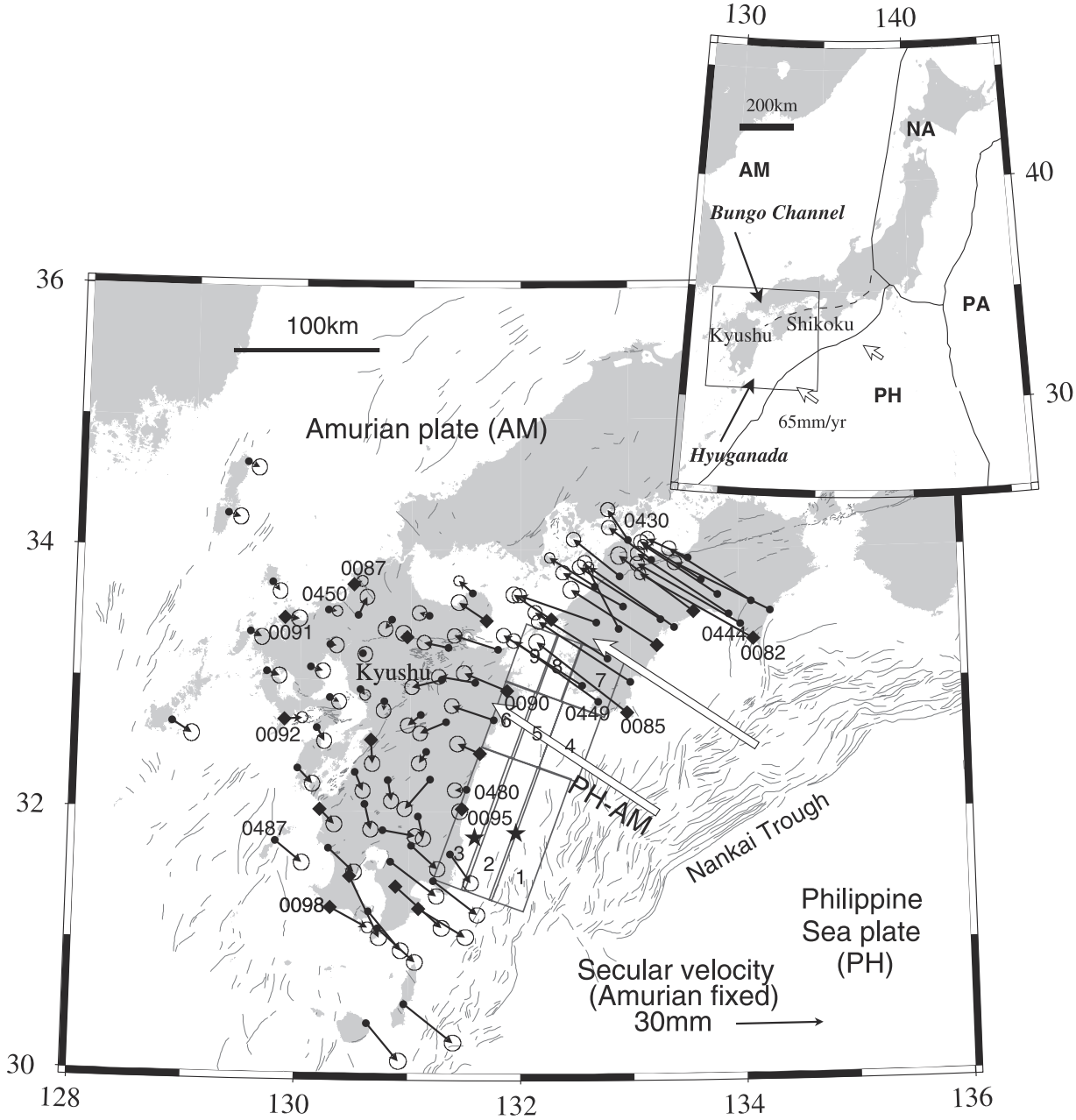

Figure 1. Tectonic setting of the Japanese islands and the GEONET station distribution in Southwest Japan. Southwest Japan, part of the Amurian plate, is overriding the Philippine Sea plate at the Nankai Trough. GEONET deploys two types of antenna-receivers, and those are processed independently, so they may have different reference frame errors. The Ashtech sites and Trimble sites are marked with diamonds and circles, respectively. The locations of specific sites referred to in the text are noted. Stars represent epicenters for the 1996 Hyuganada earthquakes that occurred on 19 October and 2 December 1996. Rectangles mark the surface projections of fault segments used in the analysis. Secular velocities are computed in ITRF96, but are displayed with respect to the stable interior of the landward, Amurian plate [e.g., *Heki et al.*, 1999], following *Miyazaki and Heki* [2001]. Error ellipses show 95% confidence regions. White vectors without error ellipses show the relative motion between the Philippine Sea and Amurian plates.

where $\mathbf{x}_{old}$, $\mathbf{x}_{new}$ are the tightly and weakly constrained positions respectively, $\Sigma_{\mathbf{x}_{old}}$, $\Sigma_{\mathbf{x}_{new}}$ are their associated covariance matrices, and A_{old}, A_{new} are the original and new constraint matrices. We used 1 m constraints for all sites, which causes the formal position uncertainties to increase to between 4 and 20 mm. An example of the deconstrained time series (only EW component) are shown in Figure 2, together with the original tightly constrained solution, where error bars are omitted for clarity. The deconstrained solutions exhibit a markedly increased

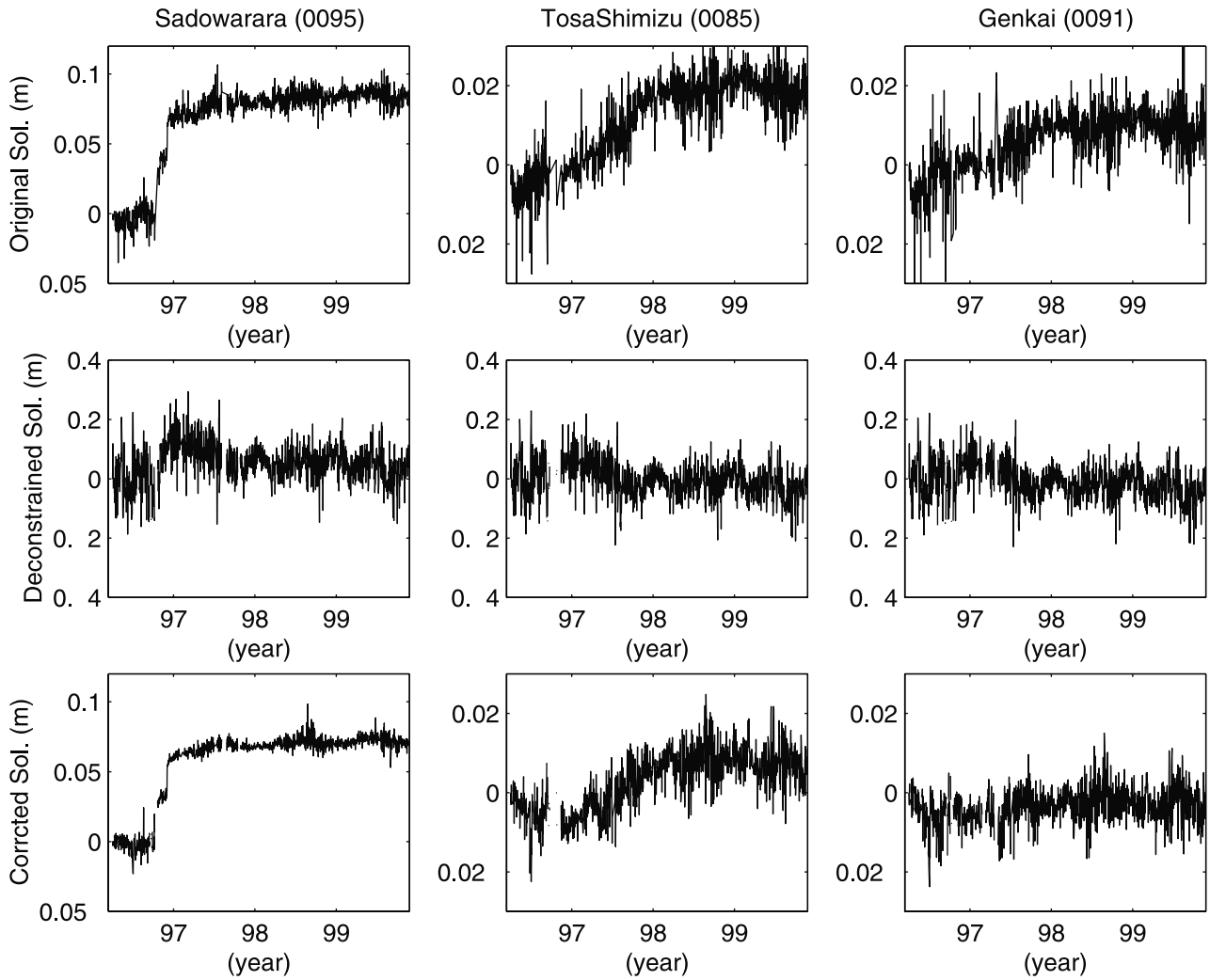

Figure 2. An example of time series for the original tightly constrained solution (top panels), for the deconstrained solution (middle panels) and the one from which the reference frame component is removed (bottom panels), for station Sadowara (0095) near the Hyuganada area, Tosa-Shimizu (0085) near the Bungo Channel, and Genkai (0091) far from the Nankai Trough. Note that the scale is different only for the deconstrained solution. Error bars are omitted for the clarity.

seasonal amplitude. *Dong* [1999] suggests that the deconstraining procedure increases the noise at the originally constrained site (Tsukuba in this case). Hence, the majority of the seasonal variation observed in the position time series may come from noise at the Tsukuba station though there may be other contributions to the seasonal variations. In the remaining analysis, we use the deconstrained solutions to reduce the effect from any inconsistency that comes from the tight constraint in the Tsukuba stations.

3. Method

[13] We employ the Network Inversion Filter [*Segall and Matthews*, 1997] to invert for transient crustal deformation. Most previous studies employ parametric methods to model transient deformation, i.e., the time series are expressed by either logarithmic [e.g., *Heki et al.*, 1997], exponential [e.g., *Yagi et al.*, 1999], or other analytic functions [e.g., *Hirose et al.*, 1999]. In contrast, the Network Inversion Filter does not assume any functional form for the time series but allows a nonparametric estimation by employing an appropriate stochastic model for the temporal evolution of fault slip. In addition, the Network Inversion Filter treats the whole network simultaneously rather than as individual time series. By analyzing the entire network simultaneously, the filter can discriminate between local time-dependent benchmark motions, and temporal variations in fault slip-rate. Hence, it is in principal possible to detect small coherent signals that are invisible in the individual time series if the network is dense enough. *Segall and Matthews* [1997] demonstrated that the filter can detect signals with signal-to-noise ratio smaller than 1.

[14] The Network Inversion Filter algorithm of *Segall and Matthews* [1997] was modified by *Segall et al.* [2000] to allow missing observations at the initial epoch. *Segall et al.* [2000] also show how to separate spatial and temporal

smoothing by implementing the spatial smoothing through pseudo-observations. This method has been applied to the postseismic deformation following the 1989 Loma Prieta Earthquake [*Segall et al.*, 2000], the 1999 Izmit earthquake [*Burgmann et al.*, 2002], and volcanic deformation accompanying the 1997 dike intrusion beneath the Izu peninsula in Japan [*Aoki et al.*, 1999]. In the present study, we utilize an extended Network Inversion Filter that accounts for reference frame errors in the GPS observations, constrains the fault thrust slip-rate to be nonnegative, and estimates the temporal and spatial smoothing parameters by including them within the state vector (McGuire and Segall, submitted manuscript, 2002).

[15] We model the GPS station positions relative to an a priori estimate $\Delta\mathbf{X}(t)$, as a function of time t, as follows

$$\Delta\mathbf{X}(t) - \mathbf{V}\cdot(t-t_0) = \sum_k H\left(t - t_{eq(k)}\right)\Delta\mathbf{X}^{cos(k)} + \int_A s_p(\xi, t-t_0)G^r_{pq}(\mathbf{x},\xi)\mathbf{n}_q(\xi)dA(\xi) + F\mathbf{f}(t) + L(\mathbf{x}, t-t_0) + \epsilon \quad (3)$$

where the left hand side represents position corrected for secular, or steady state motion. Here $\mathbf{V}$ is the secular velocity and t_0 is the reference epoch. We assume that $\Delta\mathbf{X}(t)$ and $\mathbf{V}$ are uncorrelated so that the covariance matrix for the effective data (i.e., the left hand side of (3)) is given by $\Sigma_{\mathbf{x}}(t) + \Sigma_V(t-t_0)^2$, where $\Sigma_{\mathbf{x}}(t)$ is the covariance matrix of the positions, and Σ_V is the covariance matrix of the secular velocities.

[16] The first term on right hand side represents coseismic displacements. $\Delta\mathbf{X}^{cos(k)}$ are coseismic offsets at times $t_{eq(k)}$, and $H(t)$ is a Heavyside function. The second term on the right hand side represents deformation due to transient aseismic slip. We relate the time dependent site motions to slip on faults in an elastic medium as a function of position ξ and time, $s_p(\xi, t-t_0)$ through Green's functions $G^r_{pq}(\mathbf{x}, \xi)$ in a homogeneous, isotropic, elastic half-space [e.g., *Okada*, 1985]. In (3) p, q, r = 1, 2, 3, and summation on repeated indices is implied, $\mathbf{n}_q(\xi)$ is the unit normal to the fault surface $A(\xi)$.

[17] The remaining terms are related to measurement and reference frame errors. The term $F\mathbf{f}(t)$ represent reference frame errors, where F is a linearized Helmert transformation [e.g., *Hofmann-Wellenhof et al.*, 1997] and $\mathbf{f}(t)$ is a vector of rigid body translation, rotation, and scale factor (see Appendix A). We assume that reference frame errors are uncorrelated in time and model them as a white noise process with variances appropriate for the deconstrained GSI solutions (as large as 5 m for translation, 800 mas for rotation, and 5×10^{-8} for scale). As we show below, seasonal variations observed in the data are coherent across the entire network and are largely removed by the reference frame corrections (Figure 2).

[18] The fourth term on the right hand side of (3), $L(\mathbf{x}, t - t_0)$, represents random benchmark wobble, which we model as a Brownian random walk with scale parameter τ (units length/time$^{1/2}$) [*Wyatt*, 1982, 1989]. Some studies have advocated a flicker noise model for benchmark motion [*Zhang et al.*, 1997; *Mao et al.*, 1999]. However, the observing period in these studies is at most 10 years. In addition, GPS data quality in 80s to early 90s is not satisfactory because of, e.g., inaccurate satellite information, and it is likely to have caused a high frequency noise. On the other hand, *Langbein and Johnson* [1997] using over 10 years of data show that a random walk fits the data quite well. Without a long time series it is very difficult to distinguish between flicker noise (with a $1/f$ spectral decay) and random walk (with a $1/f^2$ spectral decay). A key feature of the Network Inversion Filter is that it can distinguish spatially correlated transient signal from site specific colored noise. The reason for this is that elastic deformation causes a spatially coherent signal, whereas the local benchmark motions are, by definition, assumed to be spatially incoherent. The fact that the local benchmark motions are spatially incoherent may be more important than the precise form of the spectral decay in the time domain. Y. Aoki (personal communication, 1999) used the method of *Mao et al.* [1999] to estimate random walk parameters in the GEONET time series. He found values, on average, of about 1 mm/yr$^{1/2}$ and 4 mm/yr$^{1/2}$ for the horizontal and vertical components, respectively. *Langbein and Johnson* [1997] found similar values analyzing EDM data in California. In our analysis we assumed that the all components of all sites have the same random walk parameter, 1 mm/yr$^{1/2}$.

[19] Note that in the work of *Segall et al.* [2000], the station positions at the reference epoch, $\Delta\mathbf{X}_0$, are separate parameters from the benchmark motion, $L(\mathbf{x}, t - t_0)$, where $L(\mathbf{x}, 0) = 0$. It is more compact, however, to combine these parameters and allow the random walk to start at $\Delta\mathbf{X}_0$, $L(\mathbf{x}, 0) = \Delta\mathbf{X}_0$.

[20] The final term ϵ represents observation error, which we assume to be normally distributed with zero mean and covariance $\sigma^2\Sigma_{\mathbf{x}}$, where $\Sigma_{\mathbf{x}}$ is the covariance matrix of the deconstrained GPS positions, and σ^2 is a scale factor to account for unmodeled errors such as multipath, or azimuthally varying path delays.

4. Estimation of Reference Frame Parameters

[21] Before we apply the Network Inversion Filter, we demonstrate that the estimation of reference frame parameters at each epoch is an efficient way to eliminate common mode errors in GPS time series (For an alternate approach, see *Bock et al.* [1997] and *Wdowinski et al.* [1997]). For this purpose, we estimate only reference frame parameters and positions, and exclude aseismic slip, coseismic deformation, and benchmark wobble. In this case equation (3) reduces to

$$\Delta\mathbf{X}(t) - \mathbf{V}\cdot(t-t_0) = \Delta\mathbf{X}(t_0) + F\mathbf{f}(t) + \epsilon. \quad (4)$$

Since the two subnetworks are uncorrelated, we process each of them separately. It should be noted that the residuals to this model contain crustal deformations. This violates the assumption of the Kalman Filter that the residuals follow a Gaussian distribution. The deformation may be mapped either to benchmark wobble or to reference frame parameters, and therefore, the residual time series do not reveal the deformation accurately, and are not used in the estimation of fault slip in the following analysis.

[22] Figure 2 compares time series of the tightly constrained data, deconstrained data, and the residuals, after

Table 1. Fault Parameters for the Nankai Trough

Segment	Latitude, °	Longitude, °	*D*, km	*W*, km	*L*, km	ϕ, °	δ, °
1	31.3	131.7	35	32	120	200	17.8
2	31.4	131.5	50	32	120	200	30.8
3	31.5	131.2	70	36	120	200	38.4
4	32.3	132.2	37.5	36	60	200	16.6
5	32.4	131.9	50	28	60	200	26.4
6	32.5	131.6	70	36	60	200	37.1
7	32.8	132.4	40	40	52	200	14.6
8	32.9	132.1	50	24	52	200	23.7
9	33.0	131.9	70	36	52	200	35.9

Latitude and longitude = position of the lower right edges of the fault planes; *D* = depth of the lower edge; *W* = width; *L* = length; ϕ = strike measured clockwise from the north; δ = dip angle.

estimating and removing reference frame shifts, for three stations: Sadowara (0095), which is one of the closest stations to the epicenter of the 1996 Hyuganada earthquakes, Tosa-Shimizu (0085), which shows a significant displacement by the silent thrust event, and Genkai (0091), which is located far from the plate boundary (see Figure 1 for the locations). It is clear that much of the noise is removed by this procedure, and that the residual time series for Sadowara and Tosa-Shimizu clearly show crustal deformation associated with those events. In contrast, the

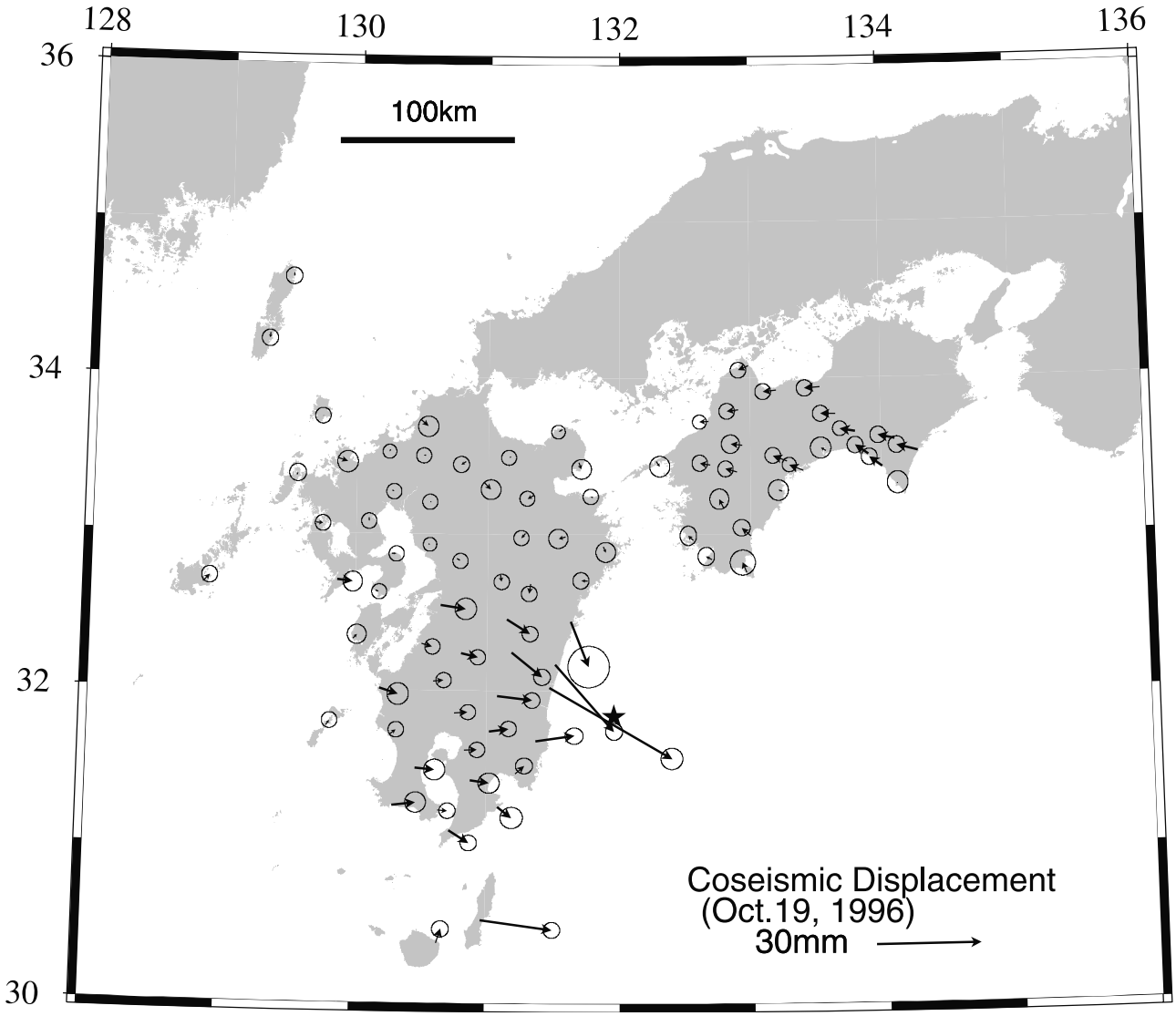

Figure 3. Coseismic displacements during the two Hyuganada earthquakes estimated by the Network Inversion Filter. (a) The 19 October 1996 event. (b) The 2 December 1996 event. Error ellipses show 95% confidence regions. Stars represent epicenters of the corresponding event.

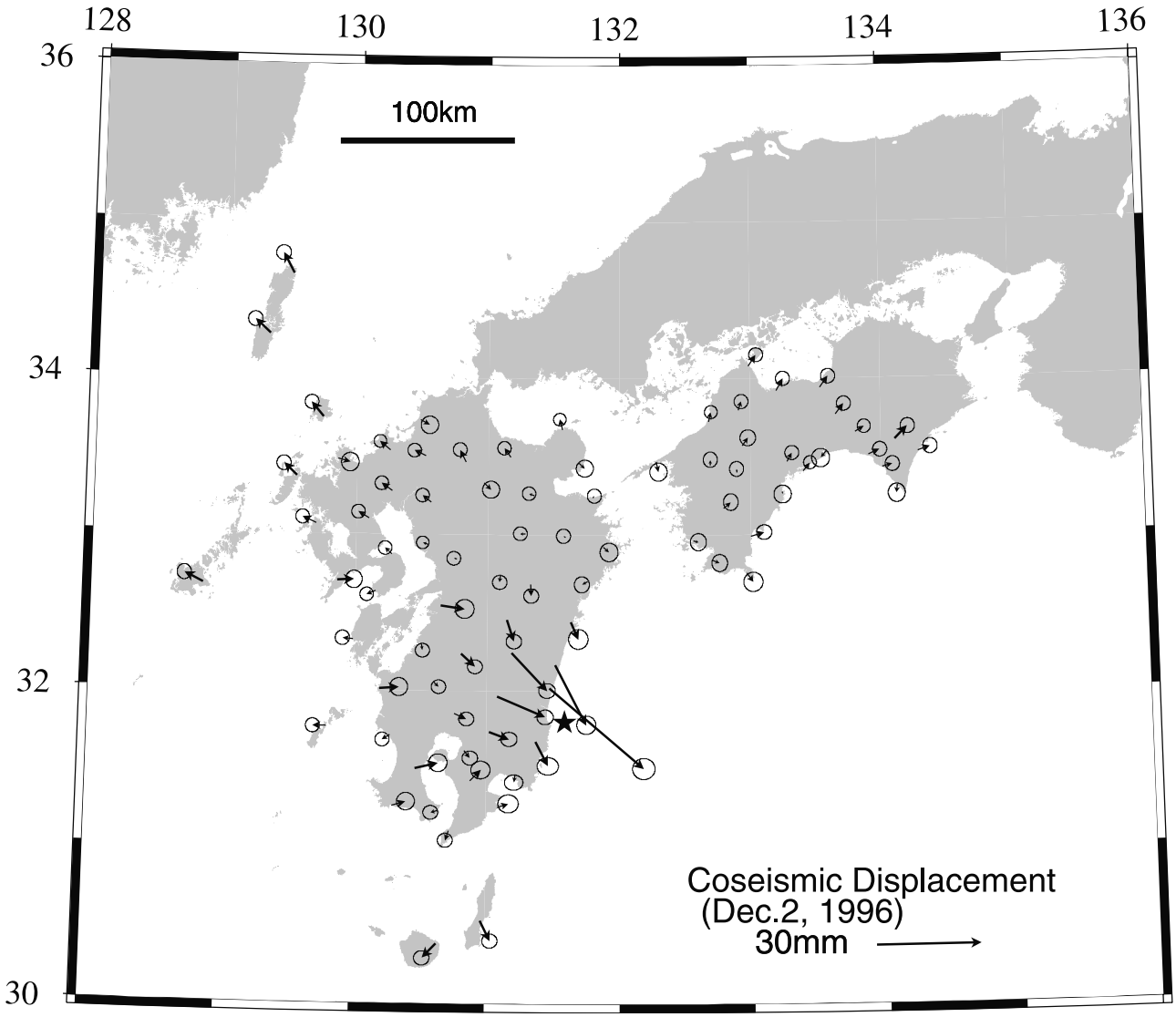

Figure 3. (continued)

residual time series for Genkai do not display transient signals suggesting that the residual time series are not biased by reference frame errors (Figure 2). These results also support our assumption that the transient signals have decayed and the deformation has returned to steady state by April 1998. In the remainder of this study, we estimate reference frame parameters simultaneously with the other model parameters.

[23] Note that for small networks it is possible to model reference frame errors as rigid body translations alone. For this network, which has dimensions of roughly 1,000 km (Tsukuba stations are included), we have found that failing to include rigid body rotations results in differences of as much as $\sim$6 mm in the estimated reference frame corrections.

5. Estimation of Secular Velocity

[24] There is not enough data prior to the first of the Hyuganada earthquakes to obtain good estimates of the secular velocity. One possible approach is to estimate the steady backslip on the Nankai trough, following *Savage* [1983]. However, part of the secular deformation is due to processes other than subduction [e.g., *Tada*, 1984, 1985], so that this approach is not fully appropriate for estimating steady state deformation. To circumvent this problem we estimate the secular velocity from the time period 1998.25 to 2000.00, which we believe to be after the important transient signals have decayed and the deformation has returned to steady state [*Hirose et al.*, 1999]. For more robust estimation of secular velocities, it is preferable to have at least 2.5–3 years of time series because of the presence of seasonal variations. Therefore, our approach is a suboptimal one to estimate secular velocities, but one that is dictated by the available data.

[25] For the secular velocity estimation, we use the deconstrained solutions, so that the absolute positions are weakly constrained. We impose a priori constraints as tight as 1 mm/yr for the horizontal velocity components at sites 0082, 0087, 0092, 0098 in the Ashtech and 0430, 0444,

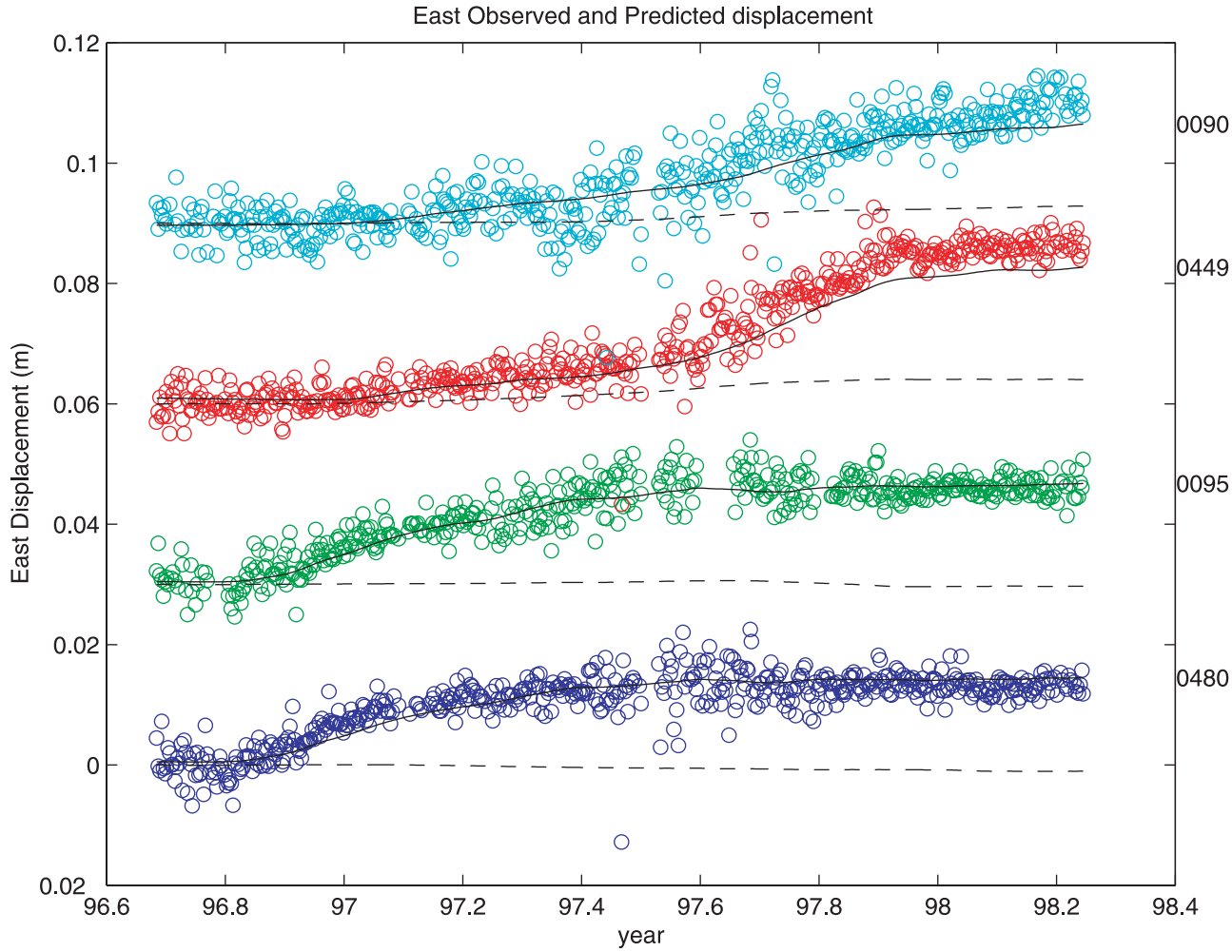

Figure 4. Fit to the data for selected stations. The data, shown as open circles, are shown corrected for coseismic steps and reference frame errors. The predicted signal components, that is component due to time dependent fault slip, and the random benchmark motion are shown with a solid line and a dashed line, respectively. (a) East components, (b) North components. see Figure 1 for station locations. Error bars, estimated to be about 6 mm horizontal and 20 mm vertical (in average), are omitted for clarity. Data uncertainties are increased by the deconstraining operation; without deconstraining the error bars would be 2 mm in horizontal components and 4 mm in the vertical.

0450, 0487 in the Trimble subnetworks (Figure 1) to their a priori values in ITRF96, leaving constraints for other components as loose as 1 m/yr and those for all site positions as large as 1 m. These constraints apply only to the estimated secular velocity and do not directly influence the inversion for time dependent slip. Since there is no correlation between Ashtech and Trimble subnetworks, we perform the velocity estimation separately for each.

[26] Observation sites on Shikoku show the effect of strong coupling at the Nankai Trough, as was pointed out in several studies [*Ozawa et al.*, 1999; *Ito et al.*, 1999; *Mazzotti et al.*, 2000; *Miyazaki and Heki*, 2001]. The situation changes rapidly as we proceed southwest to Kyushu. Although northeastern Kyushu still shows the plate interaction at the Nankai Trough, velocities in the southern part are more or less southeastward. It is presently not known whether this pattern is due to variability in plate coupling or to other processes such as back arc spreading in the Okinawa Trough [*Tada*, 1984, 1985]. In the present paper, we do not attempt to model the secular velocity field but simply subtract the velocity in ITRF96 from the deconstrained GPS data.

6. Transient Fault Slip at the Nankai Trough

[27] We performed the full network inversion filter using equation (3) and the all the available data from 4 September 1996 to 31 March 1998. The fault geometry is slightly complicated in the study area. The dip angle is only 7° to 15° off Shikoku while it is steeper off Kyushu (15° to 30°). The trough reveals a remarkable curvature in the Bungo channel. In the present paper, however, we use a simplified fault geometry using 9 rectangular fault segments as shown in Figure 1 and summarized in Table 1.

[28] Both the Hyuganada earthquakes and the silent thrust slip event are thrust events as demonstrated by their focal mechanisms [*Yagi et al.*, 1999] and estimated fault slip

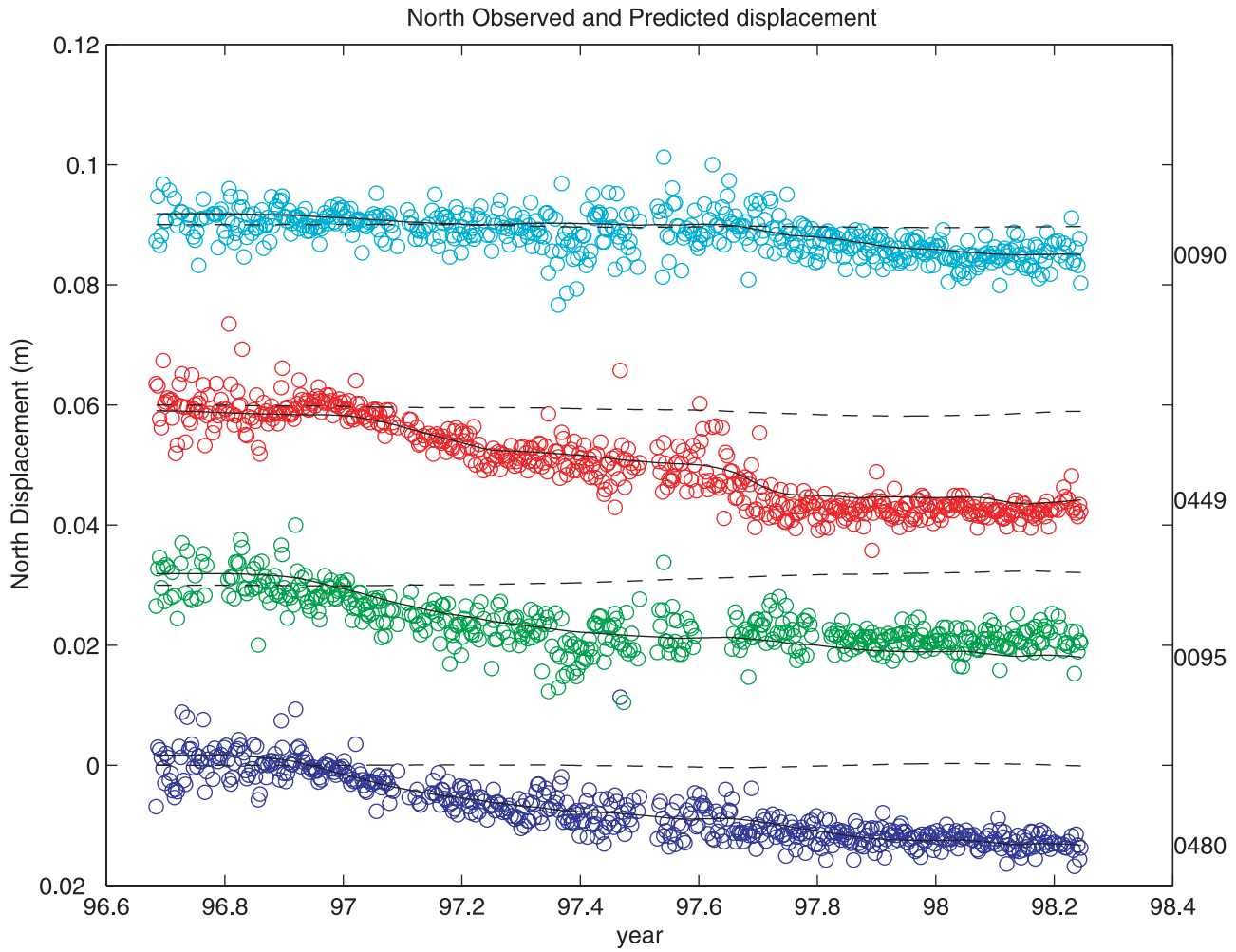

Figure 4. (continued)

distribution [*Hirose et al.*, 1999; *Ozawa et al.*, 2001]. In this case the dip slip component should be nonnegative (positive slip is defined to be reverse). Because we have already removed the contribution of secular deformation, the estimated slip distribution represents the departure from steady state. Hence, negative dip slip means a stronger coupling than the steady state coupling. The slip should never be less (more negative) than the long-term slip-rate on the megathrust. Accordingly, we regard any solution in which the minimum slip-rate is less than some value to be unphysical and impose a nonnegativity constraint using an extended Kalman filter (see McGuire and Segall, submitted manuscript, 2002).

[29] Coseismic displacements estimated by our inversion are shown in Figure 3 for the two Hyuganada earthquakes. The displacements are directed toward the trench, and decay rapidly with distance from the source regions. The fact that we do not observe significant deformation far from the epicentral region indicates that the NIF can resolve tectonic displacements from reference frame errors and random benchmark motions.

[30] Before we investigate the slip history, it is worth showing how the network inversion filter distinguished between transient deformation (signal) and site dependent benchmark motion (noise). Figure 4 shows time series of predicted signal components and local benchmark motions, together with the observations corrected for both coseismic displacements and reference frame shifts, at Saiki (0090) and Ohtsuki (0449), which are located near to one another in the northern part of the study area (Figure 1) as well as Sadowara (0095) and Kawaminami (0480), which are located near to one another in the southern part of the study area (Figure 1). Notice that the signal components of the data are quite coherent between nearby stations, whereas the local benchmark motion components are largely incoherent. Closer investigation shows some spatial coherency in the local benchmark motions. This could arise due to any number of simplifying assumptions, such as the use of homogeneous half-space elastic Green's functions, the rectangular fault planes, or by our coarse gridding of the fault. Furthermore, it may be that temporal smoothing did not allow the filter to properly track rapid changes immediately after the earthquakes, for example at Kawaminami (0480) and Sadowara (0095) in Figure 4, in which case the unmodeled postseismic deformation may have leaked into the estimated local benchmark motion. However, the amplitude of the benchmark component is only about 2 mm. The weighted-residual sum of squares, $\mathbf{r}^T \Sigma^{-1} \mathbf{r}/N_{obs} = 1.2$, if

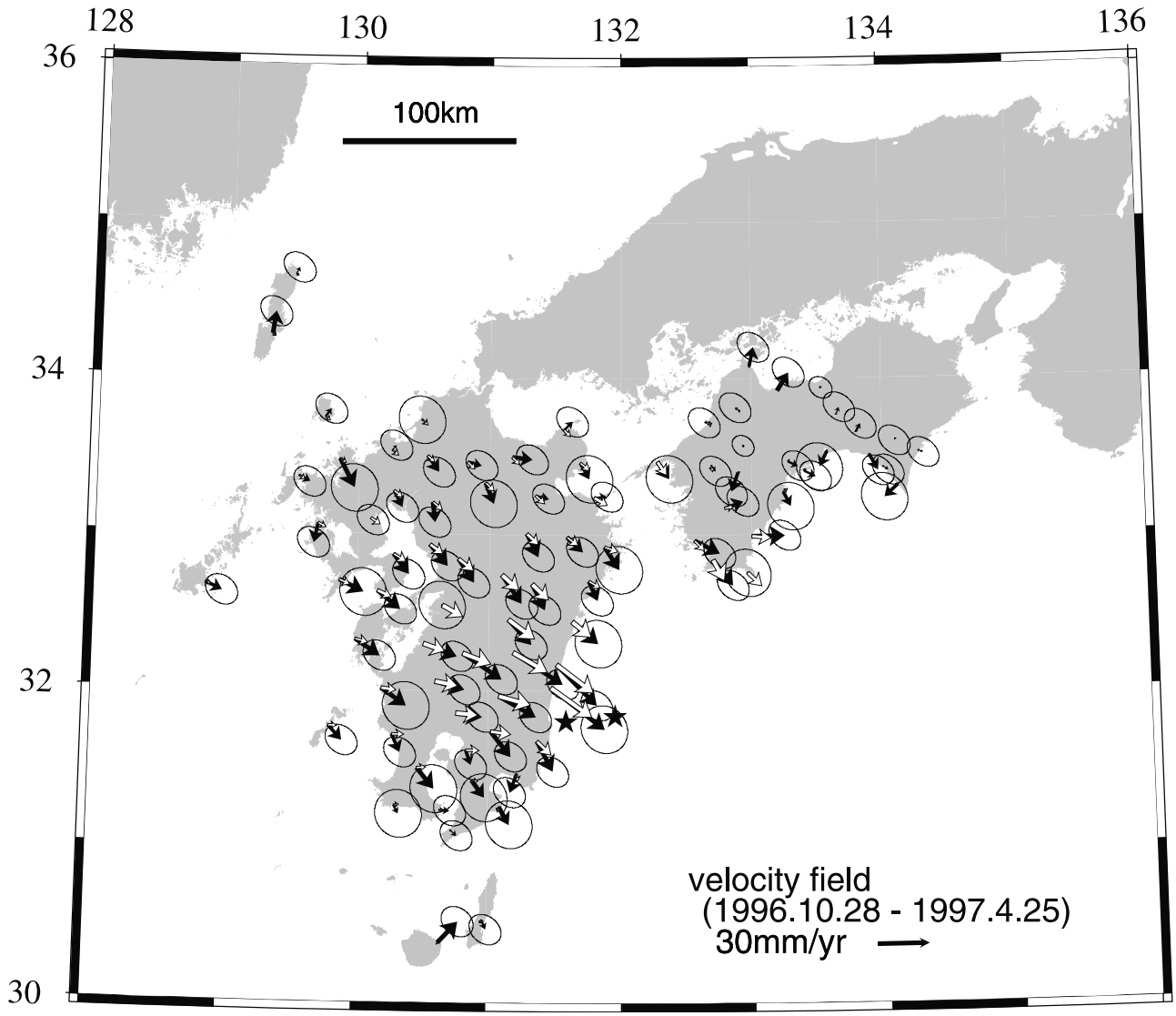

Figure 5. Time-dependent velocity field. (Departure from the secular velocity field.) Both observed (black arrows) and predicted (white arrows) velocities are shown for the periods (a) 28 October 1996–25 April 1997 and (b) 25 April 1997–19 October 1998. Error ellipses are 33% confidence regions. Note that the random benchmark motion are not included in the predicted velocity.

the random walk component is excluded from the model, and approximately 1.0 if it is included, indicating that the fit to the data is satisfactory.

[31] Figure 5 shows the average velocities (departure from the secular velocities) over two periods: 28 October 1996–25 April 1997and 25 April 1997–19 October 1998. There is significant deformation near the Hyuganada area for the first period and near the Bungo Channel for the latter period. The time-varying slip model does a reasonable good job of describing the observed motion.

[32] The space time history of fault slip-rate is shown in Figure 6. As expected for a (nonoblique) subduction zone environment (see Figure 1), the strike-slip component is substantially less than the dip-slip. Averaged over the entire fault surface, the final dip-slip is 3.5 times the final strike-slip, corresponding to a rake only 15 degrees from pure thrust. From Figure 6, postseismic slip can be seen as early as 1996.88 shortly after the first Hyuganada earthquake. After the second, deeper earthquake, afterslip appears to extend downdip (1997.1 to 1997.2). There is also an indication that shallower slip may have spread to the southwest. There is no evidence of afterslip extending to the northeast, however. Afterslip in the epicentral region of the Hyuganada earthquakes was largely complete by 1997.9.

[33] We find clear evidence for a second locus of rapid aseismic slip at the northern end of the study area which initiated beneath the southwesternmost part of Shikoku in 1997.0 roughly one month after the second Hyuganada earthquake (Figure 6). The locus of maximum slip-rate clearly migrated downdip and to the southwest. The maximum slip-rate occurred around 1997.7 and then decayed gradually until the slip event was complete by early 1998.

[34] Maximum slip-rates reach 0.6 m/yr. It must be noted, however, that the particular values depend on how the fault

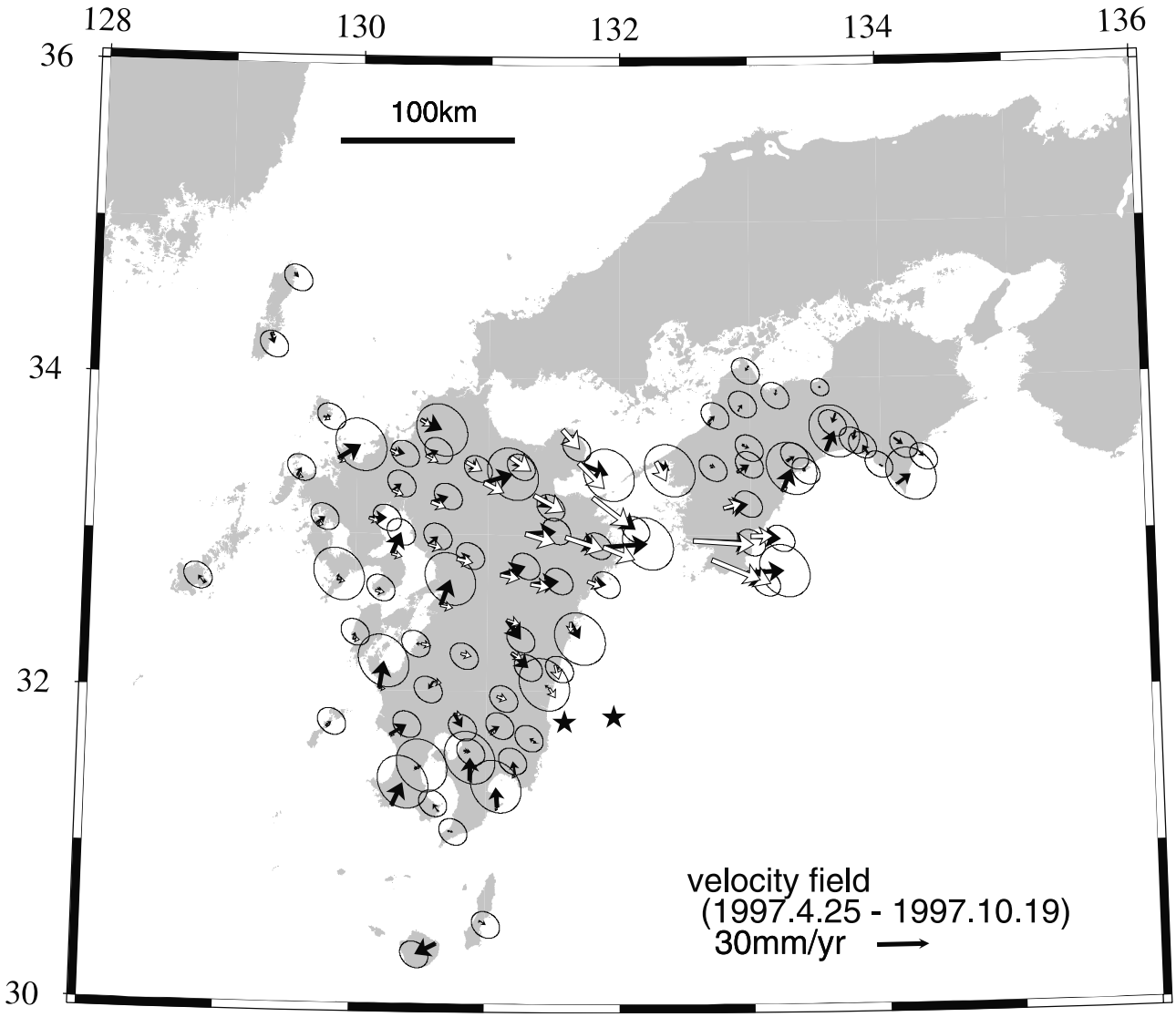

Figure 5. (continued)

surface is discretized and the degree of spatial and temporal smoothing. The formal uncertainties of the estimated slip-rates are 0.06 m/yr on average. Spatially smoother solutions exhibit largely the same character with reduced model variance.

[35] An important question is whether the slow thrust slip event is related to the postseismic deformation of the Hyuganada earthquake or it is an independent event. We do not find evidence for slip propagating from the Hyuganada area to the Bungo area; rather the two zones are separated by a part of the plate interface that did not experience anomalous slip (Figure 7). Hence, the slipping zones appear to be independent, although the slow thrust event might have been triggered by stress changes associated with the two main shocks.

7. Discussion

[36] We find no evidence that afterslip propagated over a broader region, for example from the earthquake source region to the Bungo channel. Rather, the slow thrust slip event seems to have initiated separately shortly after the second Hyuganada earthquake. *Ozawa et al.* [2001] show an apparent northward migration of slip from the Hyuganada source region toward the Bungo Channel [see *Ozawa et al.*, 2001, Figure 10]. We suggest that *Ozawa et al.* [2001] oversmoothed their solution, which causes the slip to blur between the Hyuganada and Bungo areas. Our approach includes an objective, filter-based method for choosing the spatial and temporal smoothing parameters and consistently shows that the slip in the two regions is distinct. Indeed, early inversions (not discussed here) with smoothed depleted basis functions that did not include the nonnegativity constraint, following the approach of *Segall et al.* [2000], showed similar behavior to that presented here.

[37] A second difference between our results and those of *Ozawa et al.* [2001] is that we find the silent thrust event initiated well after the second Hyuganada earthquake, whereas *Ozawa et al.* [2001] have the event starting at

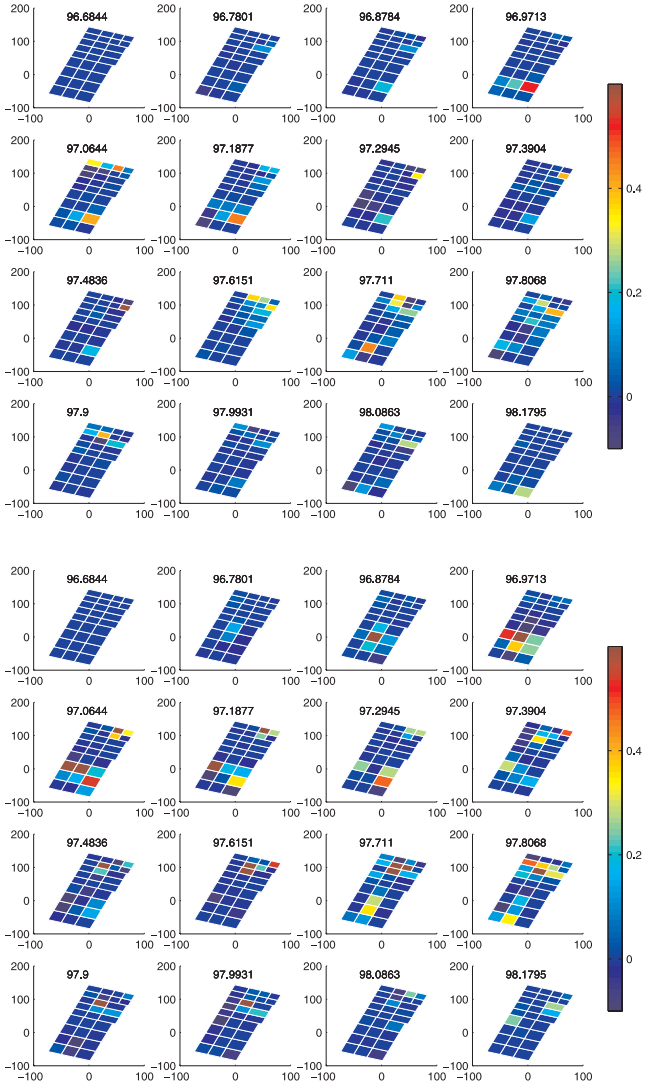

Figure 6. Spatiotemporal variation of the slip-rate. Each panel represents the slip-rate on a given day, as indicated where Day 0 corresponds to the date of the first earthquake (19 October 1996). Downdip dimension along the fault plane, and along strike distance are in km. The color scale represents the slip-rate in m/yr. (a) strike-slip. (b) dip-slip.

about the same time as the first Hyuganada earthquake. This difference is presumably due to different amounts of temporal smoothing, and emphasizes the importance of rigorous methods for determining the spatial and temporal smoothing parameters.

[38] We estimated the moment rate function for the postseismic deformation and the slow thrust slip event (Figure 8). For this calculation, slip on the southwestern half of the fault is associated with afterslip of the Hyuganada earthquakes, while slip on the remainder of the fault is associated with the silent earthquake. We find that the moment rate for postseismic deformation increases substantially following the first of the Huyganada earthquakes in 1996.8, reaches a maximum of $\sim 8 \times 10^{19}$ Nm/yr in early 1997 and then decays steadily. The accumulated moment is 3.0×10^{19} Nm and the moment magnitude is estimated to be $M_W \sim 6.9$. Since the moment magnitudes

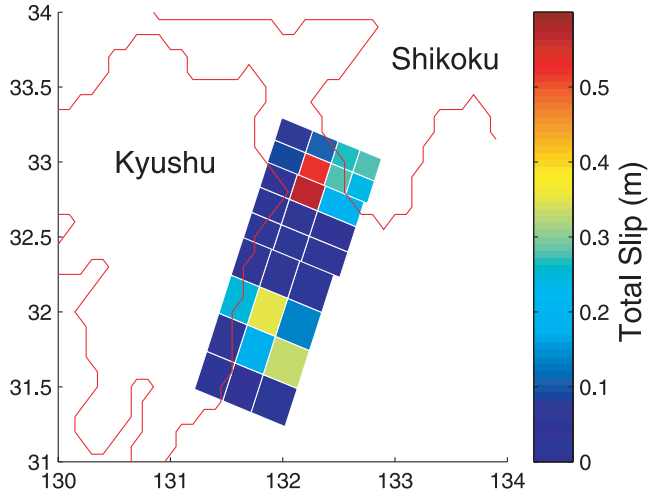

Figure 7. The total slip amplitude in excess of the secular deformation during the study period.

of two Hyuganada earthquakes were 6.7, as much strain was released by afterslip over one year as by coseismic slip.

[39] We can look in more detail at the depth distribution of aseismic afterslip in Figure 6 and Figure 9. The afterslip started at intermediate depth around the time of the first Hyuganada earthquake. The fact that the slip appears to initiate before the earthquake is presumably due to the fact that the aseismic slip is assumed to be smooth in time, not discontinuous at the time of earthquakes. Following the second, deeper Hyuganada earthquake the afterslip extended to both the deeper and shallower sections of the subduction interface. There is also a previously unidentified possible slow-slip transient in the region of the Hyuganada earthquakes around 1997.7–1997.9 that is 5.1×10^{18} Nm ($M_W \sim 6.4$). If this is the case, the Hyuganada region appears to have both aseismic afterslip

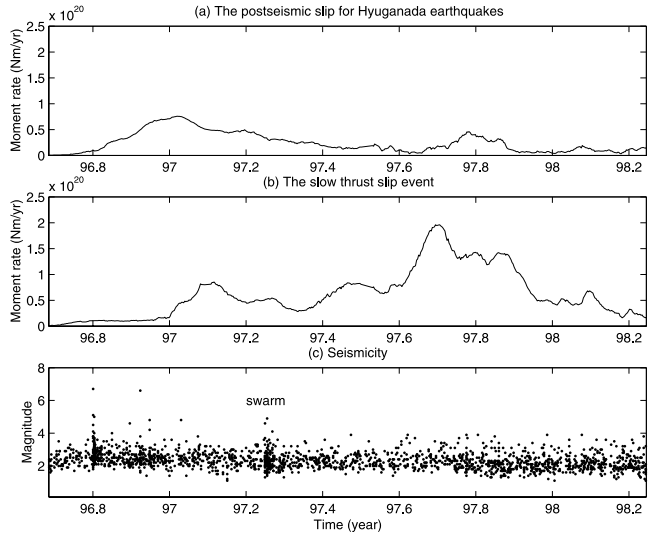

Figure 8. Seismic moment rate as a function of time for (a) the Hyuganada earthquake source region, (b) Bungo channel area, (c) Seismicity.

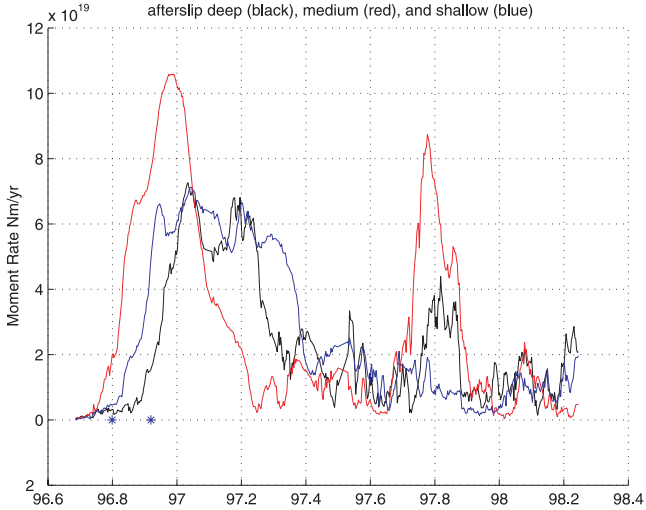

Figure 9. Temporal variation of the moment rate for the aseismic afterslip following the 1996 Hyuganada earthquakes in shallow (blue), medium (red) and deep (black) regions.

and aseismic slip transients not related to any seismic main shock.

[40] The slow thrust slip event beneath the Bungo Channel began around 1997.0 with a rapid increase in moment-release rate in the shallow portion of the thrust interface (Figure 6 and Figure 10). This initiation occurred a few weeks after the second of the Huyganada earthquakes (Figure 8). The moment rate reached $\sim 1 \times 10^{20}$ Nm/yr in early 1997 and then decayed until 1997.4. It then increased dramatically as the aseismic slip progated down-dip to the southwest in mid 1997, reaching a peak rate of nearly 2×10^{20} Nm/yr in 1997.7. The total accumulated moment, 8.1×10^{19} Nm, corresponds to $M_W \sim 7.2$. (This is larger than the previous estimate of $M_W \sim 6.6$, by *Hirose et al.* [1999], possibly because we compute the moment over the entire northern half of the model fault in our study.) If such a slow event occurred once every several tens of years, it would release the total strain accumulated over the interseismic period. It is worth noting that such transient slip events are "invisible" except by continuous geodetic measurements, and may be a key factor in explaining the discrepancy between subduction zone coupling ratios obtained by seismology and geodesy [e.g., *Shen-Tu et al.*, 1995].

[41] *Kato and Hirasawa* [1999] found from a numerical simulation based on rate and state friction laws that aseismic slip similar to the slow thrust slip event can occur if the crust has a heterogeneous distribution of friction parameters. They showed that slow slip events can occur in a rate-strengthening zone localized between two rate-weakening zones. The slow event imaged in Figure 6 occurred north of the M 7.5 1968 Hyuganada earthquake, an area that does not reveal significant slip in our inversions. These results may suggest that friction is heterogeneous on the plate boundary interface in this region. Also, the variability in slip behavior may result from complex dynamical interactions. *Yoshida and Kato* [2002] performed a numerical simulation with two degree-of-freedom block-spring model based on rate and state dependent friction laws. They classified the fault surface as either asperity, afterslip area, quasistatic episodic slip area, or interseismic slip area, in the $(b - a)\ \sigma_n - L$ plane, where a and b are coefficients in the rate and state friction equations, σ_n is normal stress, and L is a characteristic slip weakening displacement. They pointed out that slip of a block near the boundary between stable and unstable areas may occur in quasistatic events. They showed that unstable slip of one block forces the other block to displace from its equilibrium, and may cause it into quasistatic episodic slips until it gets back to equilibrium. The cumulative slip is shown to be linearly dependent on L. These results suggest the interaction of multiple sites of slip under heterogeneous frictional condition may caused such an episodic slips.

[42] *Hyndman et al.* [1995] used thermal data to infer the coupling ratio at the Nankai Trough, off Shikoku. Although they did not discuss the Hyuganada area, they classified the Bungo channel as a transition zone, between a shallower locked zone and a deeper aseismic zone. It may be that slip in these transitional areas is more likely to occur in quasistatic events, as opposed to a high-velocity ruptures.

[43] Despite its large moment release, the Bungo Channel silent earthquake had little effect on the seismicity associated with the subducting Philippine Sea Plate. The largest deviation from the background rate was a swarm of over 100 events, including 3 with $m_b > 4$, over the course of a week in early April of 1997 (Figure 8). This swarm occurred after the initiation of the Bungo Channel event, but well before the period of peak moment release (Figure 8). It is the only swarm of significant size in the Bungo Channel area between 1995 and 2001. The largest event in the swarm (m_b 4.9) had a normal faulting focal mechanism indicating that the swarm probably occurred in the subducted oceanic crust rather than on the thrust interface. Thus, despite the large strain rate and associated stress changes on the deeper part of the thrust

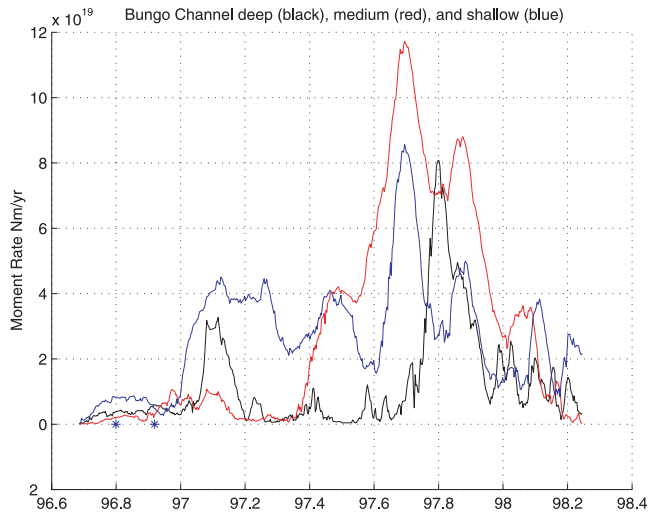

Figure 10. Temporal variation of the moment rate for the slow event at Bungo Channel in shallow (blue), medium (red) and deep (black) regions.

interface, no significant inertia dominated instabilities were generated.

8. Conclusion

[44] We investigated the spatiotemporal variation of fault slip beneath the Nankai Trough off southwest Japan for 1.5 years following the 1996 Hyuganada earthquakes. Afterslip was concentrated near the hypocenter of the first Hyuganada earthquake, but north of the second quake. The cumulative moment released by afterslip was about 3.0×10^{19} Nm, approximately the same as that released by the high-velocity ruptures. We also image a slow thrust slip event beneath the Bungo Channel. The slow slip initiated about one month after the second Hyuganada earthquake beneath the southwestern part of Shikoku island. The slipping zone then propagated to the southwest and grew slowly over the next 6 months. Finally, the slip decelerated over the following 6 months. The cumulative moment released by the slow thrust slip event was about 8.1×10^{19} Nm, approximately the same as a M7 class earthquake. We find no evidence that afterslip from the Hyuganada earthquakes propagated to the north initiating the Bungo channel slow event. The source region of the slow thrust slip event, may mark a boundary between strong and weakly coupled plate interface. Variations in fault zone constitutive properties may account for these differences and for the unusual character of the slow event. Other, previously undetected, slow slip events may account for substantial release of accumulated elastic strain.

Appendix A: Reference Frame Correction

[45] The reference frame correction is simply added to the general Network Inversion Filter architecture. In the observation equation (3) the matrix F relating the frame parameters to the data contains submatricies corresponding to reference frame translation, rotation, and scale, given by

$$F_{tr} = \begin{bmatrix} 1 & 1 & 1 \\ \vdots & \vdots & \vdots \\ 1 & 1 & 1 \end{bmatrix}, F_{ro} = \begin{bmatrix} R(\mathbf{X}_1(t_0)) \\ \vdots \\ R(\mathbf{X}_N(t_0)) \end{bmatrix}, F_{sc} = \begin{bmatrix} \mathbf{X}_1(t_0) \\ \vdots \\ \mathbf{X}_N(t_0) \end{bmatrix}. \quad \text{(A1)}$$

Here R corresponds to a rotation matrix given by

$$R = \begin{bmatrix} 0 & -z_0 & y_0 \\ z_0 & 0 & -x_0 \\ -y_0 & x_0 & 0 \end{bmatrix} \quad \text{(A2)}$$

in which $\mathbf{X}_N = (x_0, y_0, z_0)$ represents the a priori coordinates of the N-th station.

[46] We assume that the reference frame errors are uncorrelated from epoch to epoch. Thus, in the state evolution equation [see *Segall and Matthews*, 1997] the state transition matrix contains a submatrix of zeros. The corresponding process noise matrix contains an identity submatrix scaled by the frame variance σ_f^2.

[47] **Acknowledgments.** We thank the Geographical Survey Institute for providing their GPS solutions in SINEX format, Satoshi Ide for providing the seismic catalog. We also thank Danan Dong, Mark Murray, Yosuke Aoki, Shinzaburo Ozawa, Yuji Yagi, and Hitoshi Hirose for their valuable comments, suggestions, and discussions. Critical reviews by an anonymous associate editor, Y. Fialko (SIO), and an anonymous reviewer significantly improved the quality of this manuscript. This study was done during S.M.'s stay at Stanford University, supported by The Long-Term Scholarship Program of the Science and Technology Agency, Government of Japan. A software package, Generic Mapping Tool (GMT), was used to plot the figures [*Wessel and Smith*, 1995].

References

Ando, M., Source mechanisms and tectonic significance of historical earthquakes along the Nankai Trough, Japan, *Tectonophysics*, *27*, 119–140, 1975.

Aoki, Y., P. Segall, T. Kato, P. Cervelli, and S. Shimada, Imaging magma transport during the 1997 seismic swarm off the Izu Peninsula, Japan, *Science*, *286*, 927–930, 1999.

Bock, Y., et al., Southern California permanent GPS geodetic array: Continuous measurements of regional crustal deformation between the 1992 Landers and 1994 Northridge earthquakes, *J. Geophys. Res.*, *102*, 18,013–18,033, 1997.

Burgmann, R., S. Ergintav, P. Segall, L. Hearn, S. McClusky, R. E. Reilinger, H. Woith, and J. Zschau, Time–space variable afterslip on and deep below the Izmit earthquake rupture, *Bull. Seismol. Soc. Am.*, *92*, 126–137, 2002.

Dong, D., *Quasi-Observation Calculation Analysis (QOCA)*, Jet Propol. Lab., Pasadena, Calif., 1999. (Available at http:/gipsy.jpl.nasa.gov/qoca)

Dong, D., T. A. Herring, and R. W. King, Estimating regional deformation from a combination of space and terrestrial geodetic data, *J. Geod.*, *72*, 200–214, 1998.

Dong, D., P. Fang, Y. Bock, M. K. Cheng, and S. Miyazaki, Anatomy of apparent seasonal variations from GPS-derived site position time series, *J. Geophys. Res.*, *107*(B4), 2075, doi:10.1029/2001JB000573, 2002.

Heki, K., S. Miyazaki, and H. Tsuji, Silent fault slip following an interplate earthquake at the Japan Trench, *Nature*, *386*, 595–598, 1997.

Heki, K., S. Miyazaki, H. Takahashi, M. Kasahara, F. Kimata, S. Miura, N. F. Vasilenko, A. Ivashchenko, and K. An, The Amurian plate motion and current plate kinematics in eastern Asia, *J. Geophys. Res.*, *104*, 29,147–29,155, 1999.

Hirose, H., K. Hirahara, F. Kimata, N. Fujii, and S. Miyazaki, A slow thrust slip event following the two 1996 Hyuganada earthquakes beneath the Bungo Channel, southwest Japan, *Geophys. Res. Lett.*, *26*, 3237–3240, 1999.

Hofmann-Wellenhof, B., H. Lichtenegger, and J. Collins, *GPS: Theory and Practice*, 4th ed., Springer-Verlag, New York, 1997.

Hyndman, R. D., K. Wang, and M. Yamano, Thermal constraints on the seismogenic portion of the southwestern Japan subduction thrust, *J. Geophys. Res.*, *100*, 15,373–15,392, 1995.

Ito, T., S. Yoshioka, and S. Miyazaki, Interplate coupling in southwest Japan deduced from inversion analysis of GPS data, *Phys. Earth Planet. Inter.*, *115*, 17–34, 1999.

Kato, N., and T. Hirasawa, Nonuniform and unsteady sliding of a plate boundary in a great earthquake cycle: A numerical simulation using a laboratory-derived friction law, *Pure Appl. Geophys.*, *155*, 93–118, 1999.

Kumagai, H., Time sequence and the recurrence models for large earthquakes along the Nankai Trough revisited, *Geophys. Res. Lett.*, *23*, 1139–1142, 1996.

Langbein, J., and H. Johnson, Correlated errors in geodetic time series: Implications for time-dependent deformation, *J. Geophys. Res.*, *102*, 591–603, 1997.

Mao, A., C. G. A. Harrison, and T. H. Dixon, Noise in GPS coordinate time series, *J. Geophys. Res.*, *104*, 2797–2816, 1999.

Mazzotti, S., X. Le Pichon, P. Henry, and S. Miyazaki, Full interseismic locking of the Nankai and Japan–West Kurile subduction zones: An analysis of uniform elastic strain accumulation in Japan constrained by permanent GPS, *J. Geophys. Res.*, *105*, 13,159–13,177, 2000.

Miyazaki, S., and K. Heki, Crustal velocity field of southwest Japan: Subduction and arc-arc collision, *J. Geophys. Res.*, *106*, 4305–4326, 2001.

Miyazaki, S., T. Saito, M. Sasaki, Y. Hatanaka, and Y. Iimura, Expansion of GSI's nationwide GPS array, *Bull. Geogr. Surv. Inst.*, *43*, 23–34, 1997.

Okada, Y., Surface deformation due to shear and tensile faults in a half-space, *Bull. Seismol. Soc. Am.*, *75*, 1135–1154, 1985.

Ozawa, S., M. Murakami, and T. Tada, Time-dependent inversion study of the slow thrust event in the Nankai trough subduction zone, southwest Japan, *J. Geophys. Res.*, *106*, 787–803, 2001.

Ozawa, T., T. Tabei, and S. Miyazaki, Interplate coupling along the Nankai Trough off southwest Japan derived from GPS measurements, *Geophys. Res. Lett.*, *26*, 927–930, 1999.

Rothacher, M., and L. Marvert, *Bernese GPS Software Version 4.0*, Univ. of Berne, Berne, Switzerland, 1996.

Sangawa, A., The paleo-earthquake study using traces of the liquefaction (in Japanese), *Quat. Res.*, *32*, 249–255, 1993.

Savage, J. C., A dislocation model of strain accumulation and release at a subduction zone, *J. Geophys. Res.*, *88*, 4984–4996, 1983.

Segall, P., and M. Matthews, Time dependent inversion of geodetic data, *J. Geophys. Res.*, *102*, 22,391–22,400, 1997.

Segall, P., R. Burgmann, and M. Matthews, Time-dependent triggered afterslip following the 1989 Loma Prieta earthquake, *J. Geophys. Res.*, *105*, 5615–5634, 2000.

Shen-Tu, B., W. E. Holt, and A. J. Haines, Intraplate deformation in the Japanese Islands: A kinematic study of intraplate deformation at a convergent plate margin, *J. Geophys. Res.*, *100*, 24,275–24,293, 1995.

Shiono, K., T. Mikumo, and Y. Ishikawa, Tectonics of the Kyushu–Ryukyu arc as evidenced from seismicity and focal mechanism of shallow to intermediate-depth earthquakes, *J. Phys. Earth*, *28*, 17–43, 1980.

Sillard, P., Z. Altamimi, and C. Boucher, The ITRF96 realization and its associated velocity field, *Geophys. Res. Lett.*, *25*, 3223–3226, 1998.

Tada, T., Spreading of the Okinawa trough and its relation to the crustal deformation in Kyushu (in Japanese with English abstract), *Zisin*, *37*, 407–415, 1984.

Tada, T., Spreading of the Okinawa trough and its relation to the crustal deformation in Kyushu, 2 (in Japanese with English abstract), *Zisin*, *38*, 1–12, 1985.

Tsuji, H., Y. Hatanaka, T. Sagiya, and M. Hashimoto, Coseismic crustal deformation from the 1994 Hokkaido–Toho–Oki earthquake monitored by a nationwide continuous GPS array in Japan, *Geophys. Res. Lett.*, *22*, 1669–1672, 1995.

Wdowinski, S., Y. Bock, J. Zhang, P. Fang, and J. Genrich, Southern California permanent GPS geodetic array: Spatial filtering of daily positions for estimating coseismic and postseismic displacements induced by the 1992 Landers earthquake, *J. Geophys. Res.*, *102*, 18,057–18,070, 1997.

Wessel, P., and W. H. F. Smith, New version of the Generic Mapping Tools released, *Eos Trans. AGU*, *76*33, 329–330, 1995.

Wyatt, F. K., Displacement of surface monumentations: Horizontal motion, *J. Geophys. Res.*, *87*, 979–989, 1982.

Wyatt, F. K., Displacement of surface monumentations: Vertical motion, *J. Geophys. Res.*, *94*, 1655–1664, 1989.

Yagi, Y., M. Kikuchi, S. Yoshida, and T. Sagiya, Comparison of the coseismic rupture with the aftershock distribution in the Hyuga-nada earthquakes of 1996, *Geophys. Res. Lett.*, *26*, 3161–3164, 1999.

Yagi, Y., M. Kikuchi, and T. Sagiya, Co-seismic slip, post-seismic slip, and aftershocks associated with two large earthquakes in 1996 in Hyuganada, Japan, *Earth Planets Space*, *53*, 793–803, 2001.

Yoshida, S., and N. Kato, Episodic slip in two degree-of-freedom blockspring model, paper presented at Joint Meeting of Earth and Planetary Science, Joint Meet. Org. Off., Tokyo, 2002.

Zhang, J., Y. Bock, H. Johnson, P. Fang, S. Williams, J. Genrich, S. Wdowinski, and J. Behr, Southern California permanent GPS geodetic array: Error analysis of daily position estimates and site velocities, *J. Geophys. Res.*, *102*, 18,035–18,055, 1997.

J. J. McGuire, Department of Geology and Geophysics, Woods Hole Oceanographic Institution, Woods Hole, MA 02543, USA. (jmcguire@whoi.edu)

S. Miyazaki, Earthquake Research Institute, University of Tokyo, 1-1, Yayoi-1, Bunkyo-ku, Tokyo 113-0032, Japan. (miyazaki@eri.u-tokyo.ac.jp)

P. Segall, Department of Geophysics, Stanford University, Stanford, CA 94305, USA. (segall@stanford.edu)